Coordination of Actinide Ions in Wells−Dawson Heteropolyoxoanion Complexes

Ming-Hsi Chiang,[a] Clayton W. Williams,[a] L. Soderholm,*[a] and Mark R. Antonio*[a]

Keywords: Actinides / Electrostatic interactions / Lanthanides / Polyoxometalates / X-ray absorption spectroscopy

Although many low-valent (III, IV) actinide (An) ions are known to form coordination complexes with the α-2 isomer of the lacunary Wells–Dawson polyoxoanion, $[P_2W_{17}O_{61}]^{10-}$, there is little structural information about the An–O interactions, particularly in solution. We have probed the An–O coordination environment for the series of clusters $[An(\alpha\text{-}2\text{-}P_2W_{17}O_{61})_2]^{n-}$ with An^{4+} (Th^{4+}, U^{4+}, Np^{4+}, Pu^{4+}) and An^{3+} (Np^{3+}, Pu^{3+}, Am^{3+}) in both solution and solid phases using X-ray absorption fine structure (XAFS). Comparisons are made with the lanthanide (Ln) coordination environments in the series of 4*f*-ion clusters, $[Ln^{n+}(\alpha\text{-}2\text{-}P_2W_{17}O_{61})_2]^{n-20}$, and with the related monovacant Lindqvist anions, $[Ln^{n+}(W_5O_{18})_2]^{n-12}$, for $n = 3, 4$. The average An–O_8 and Ln–O_8 distances correlate with their cationic VIII-coordinate ionic radii, indicating that the An and Ln ions have indistinguishable coordination behavior. Metrical details are consistent with simple charge and size considerations for both trivalent and tetravalent An ions as well as Ln ions coordinated with α-2-$[P_2W_{17}O_{61}]^{10-}$ and $[W_5O_{18}]^{6-}$. This result is contrasted to trends established for these *f*-ions coordinated to the Preyssler anion $[Ln^{n+}P_5W_{30}O_{110}]^{n-15}$.

Introduction

A significant body of international work demonstrates that polyoxometalates like the lacunary monovacant Wells−Dawson anion $[P_2W_{17}O_{61}]^{10-}$ act as stabilizing chelators of tetravalent actinide (An) ions.[1] The stabilization of these otherwise-reactive cations of uranium and the *trans*-U elements provides the basis for the application of polyoxoanions to selected aspects of An separations science in nuclear waste processing.[2] One recent practical application conceived at the CEA (Commissariat à l'Energie Atomique − France) concerns the use of α-2-$[P_2W_{17}O_{61}]^{10-}$ as a reagent for the confinement and off-line analysis of U^{4+} as part of the plutonium recovery process known as PUREX.[3,4] Another application advanced by the CEA to separate Am^{3+} from Cm^{3+} and trivalent lanthanide (Ln) elements involves its selective oxidation to Am^{4+} in the presence of α-2-$[P_2W_{17}O_{61}]^{10-}$ followed by solvent extraction. In this process, known as SESAME,[5,6] neither Cm^{3+} nor Ln^{3+} (except Ce) are oxidized thereby facilitating their separation from Am^{4+} as a valence-stabilized complex of α-2-$[P_2W_{17}O_{61}]^{10-}$. In research at JAERI (Japan Atomic Energy Research Institute), the process known as PARC is similarly planned to exploit the chemistry of α-2-$[P_2W_{17}O_{61}]^{10-}$ for separation of Am.[7] These applications are driven by the oxidizing power of α-2-$[P_2W_{17}O_{61}]^{10-}$ and its coordination chemistry, specifically its service as a valence-controlling complexant.

Despite current practice and future promise, there are few metrical details about the coordination of An^{4+} ions in complexes with α-2-$[P_2W_{17}O_{61}]^{10-}$. Such information would provide insights about the strength and nature of the An-ligand interactions. A large collection of previous work has shown that An^{4+} ions are strongly chelated by the α-2-$[P_2W_{17}O_{61}]^{10-}$ anion in butterfly-like complexes with 1:2 stoichiometry wherein one An cation is coordinated between two α-2-$[P_2W_{17}O_{61}]^{10-}$ anions. Although there is considerable physical and spectroscopic evidence for clusters of the general form $[An(\alpha\text{-}2\text{-}P_2W_{17}O_{61})_2]^{n-}$ ($n = 16$ for An^{4+}, and $n = 17$ for An^{3+}),[1,4,8] no complete crystal structures are available.[9] The combination of results from exhaustive studies of the coordination chemistry of U^{4+} in $[U(\alpha\text{-}2\text{-}P_2W_{17}O_{61})_2]^{16-}$ both in the solid state and in aqueous solution indicates a square antiprismatic environment of 8 O about U.[4] The oxophilic *trans*-uranium elements are assumed to maintain this same coordination environment throughout the 5*f* series of $[An(\alpha\text{-}2\text{-}P_2W_{17}O_{61})_2]^{n-}$ complexes. Similar, albeit weaker, complexation with the trivalent actinides is also known.[10] The crystal structures of the lanthanide clusters $[Lu(\alpha\text{-}2\text{-}P_2W_{17}O_{61})_2]^{17-}$ and $[Ce(\alpha\text{-}2\text{-}P_2W_{17}O_{61})_2]^{16-}$ reveal eight-coordinate square antiprism geometries for both Lu^{3+} and Ce^{4+}.[11,12] The common structure is illustrated in Figure 1(a). It shows that the central 4*f*-ion is coordinated to 2 α-2-$[P_2W_{17}O_{61}]^{10-}$ anions in a *syn* conformation through 4 O atoms on each.

[a] Chemistry Division, Argonne National Laboratory,
9700 South Cass Avenue, Argonne, IL 60439-4831, USA
Fax: (internat.) + 1-630/252-4225
E-mail: ls@anl.gov
mantonio@anl.gov

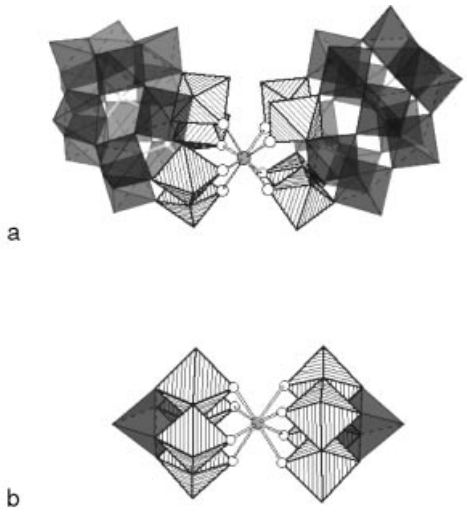

Figure 1. Molecular structures of (a) $[Lu(\alpha\text{-}2\text{-}P_2W_{17}O_{61})_2]^{17-}$ [11] and (b) $[Np(W_5O_{18})_2]^{8-}$ [13] that emphasize the square antiprism oxygen coordination environments of the Lu^{3+} (IR = 0.977 Å) and Np^{4+} (IR = 0.98 Å) ions, depicted as the central solid circles. The striped WO_6 octahedra contain the O atoms, depicted as open circles, that bind the Ln and An ions. The shaded WO_6 polygons complete the ligand structures

Insights about the structural aspects of An−O coordination and its influence on the stability of the An^{4+} complexes are what interest us for both fundamental and practical reasons. In order to probe An^{4+}−O bonding and stabilization throughout the 5*f*-series of complexes $[An(\alpha\text{-}2\text{-}P_2W_{17}O_{61})_2]^{16-}$ for An ≡ Th, U, Np, Pu we report the An L_3-edge XANES (X-ray absorption near edge structure) and EXAFS (extended X-ray absorption fine structure). These techniques provide access to a quantitative understanding of the An−O coordination for the solution specimens generated under electrochemical control and for the poorly-crystalline solids examined herein, for which conventional molecular level measurements like X-ray diffraction can be problematic. The results are compared with those for the An^{3+} complexes of $[An(\alpha\text{-}2\text{-}P_2W_{17}O_{61})_2]^{17-}$ for An ≡ Np, Pu, Am, and discussed in light of available metrical information for Ln^{3+} polyoxoanion complexes of $\alpha\text{-}2\text{-}[P_2W_{17}O_{61}]^{10-}$ and $[W_5O_{18}]^{6-}$. This latter tungsten oxide is known as the monovacant Lindqvist isopolyoxoanion. It binds tetravalent An as well as trivalent and tetravalent Ln ions to form complexes of 1:2 stoichiometry, $[An(W_5O_{18})_2]^{8-}$ and $[Ln^{n+}(W_5O_{18})_2]^{n-12}$. Many crystal structures have been determined of the actinide[13−15] and lanthanide[16−24] decatungstate clusters, as typified by the illustration in Figure 1(b). The direct comparisons of the An^{4+}−O and An^{3+}−O bonding in terms of interatomic distances provides an atomic-level perspective of the An coordination environments in polyoxometalates.

Results and Discussion

The An L_3 XANES data for the solid salts and aqueous solutions of the $[An(\alpha\text{-}2\text{-}P_2W_{17}O_{61})_2]^{n-}$ anions are shown in Figure 2. All spectra reveal a steeply rising edge peak whose position is diagnostic of the An oxidation state. The U, Np, and Pu solution XANES collected at rest potential all have edge energies consistent with An^{4+}. After obtaining these spectra, the Np and Pu samples were electrochemically reduced in situ, and the XANES spectra were recorded of the blue solutions held at reducing potentials. These data, shown as the dashed lines in Figure 2, have edge energies shifted with respect to the data obtained at rest potential. Analyses of the edge positions indicate that both Np^{4+} and Pu^{4+} have been reduced to An^{3+}. The 4.6 and 4.3 eV differences between the $Np^{4+} - Np^{3+}$ and $Pu^{4+} - Pu^{3+}$ edge peak positions of Table 1 attest to the An^{4+}/An^{3+} redox activity in the clusters, which is an independent subject of interest.[1] The edge resonances and their shifts with oxidation state are consistent with previous work on the trivalent and tetravalent An ions.[25,26] The results from the fits to the XANES spectra, including peak positions, line widths, and intensities, are detailed in Table 1.

The L_3-edge $k^3\chi(k)$ EXAFS for the heteropolyoxoanion complexes with An^{3+} and An^{4+} is shown in the left panels of Figure 3 as solid lines. These data were Fourier trans-

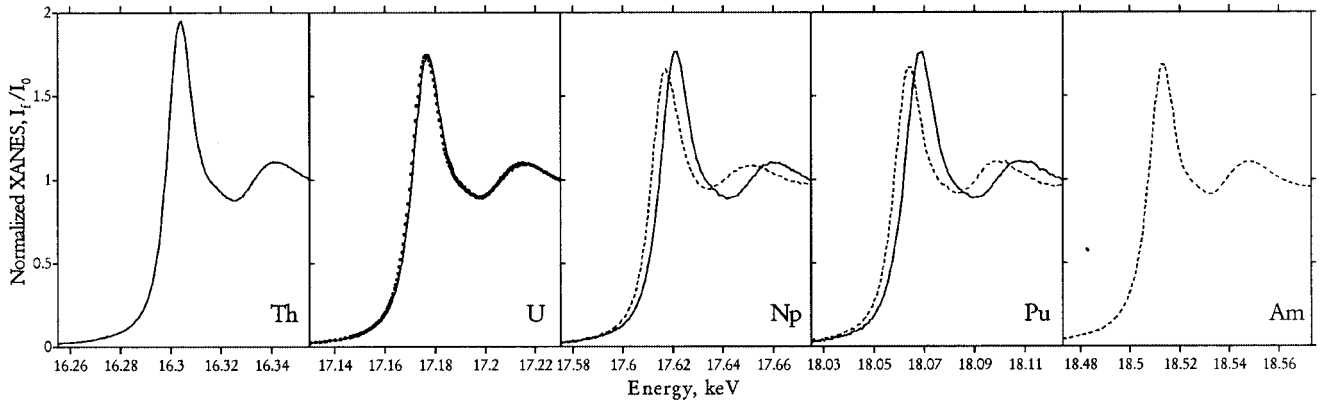

Figure 2. Normalized fluorescence L_3-edge XANES for the series of clusters $[An(\alpha\text{-}2\text{-}P_2W_{17}O_{61})_2]^{n-}$ with An of, in left to right panel order, Th; U; Np; Pu; Am. The An^{4+} and An^{3+} spectra are shown as solid and dashed lines, respectively. All Np and Pu XANES spectra were obtained as solution samples. Th and Am XANES were obtained as solid samples, and the U spectra were obtained as both solution and solid samples, shown here with open circles and a solid line, respectively

Table 1. Ionic radii (IR) and physical forms of the $[An(\alpha\text{-}2\text{-}P_2W_{17}O_{61})_2]^{n-}$ complexes with An^{4+} (Th, U, Np, Pu) and An^{3+} (Np, Pu, Am). Inflection points from the first differential L_3-edge Th, U, Np, Pu, and Am XANES and results − positions (eV), widths (eV), and heights − from curve fitting to the normalized XANES of Figure 2 with one Gaussian peak shape and one arctangent function. Estimated error for positions and widths, ±0.5 eV; all arctangent heights, 1.00±0.01

An	Th^{4+}	U^{4+}		Np^{4+}	Np^{3+} [b]	Pu^{4+}	Pu^{3+} [b]	Am^{3+}
IR, CN=VIII[a]	1.05	1.00		0.98	1.12	0.96	1.10	1.09
Color/Phase	white/solid	violet/solution	violet/solid	yellow/solution	blue/solution	pink/solution	blue/solution	orange/solid
Inflection Point	16299.7	17171.5	17171.7	17616.1	17611.5	18063.1	18058.8	18508.4
Gaussian Position	16303.9	17175.9	17176.5	17620.3	17616.1	18067.6	18063.1	18513.2
Gaussian FWHM	12.3	15.5	15.5	16.1	15.7	16.9	15.2	11.9
Gaussian Height	1.10	0.98	0.97	1.04	0.84	1.08	0.93	0.83
Arctan energy	16296.0	17171.1	17171.4	17616.5	17611.5	18065.4	18059.7	18503.8
Arctan FWHM	15.9	19.3	18.9	20.1	16.0	20.5	17.9	15.6

[a] Obtained from Shannon[27] for coordination number (CN) 8. [b] XAFS data for the heteropoly blues of $[An^{3+}(\alpha\text{-}2\text{-}P_2W_{17}O_{61})_2]^{n-}$ with Np and Pu collected in situ following exhaustive electrolysis at −1.00 V and −0.30 V, respectively, vs. Ag/AgCl.

Table 2. Metrical results − oxygen coordination number, An−O interatomic distance and Debye−Waller (DW) factor, and energy shift − obtained from curve fitting the Th, U, Np, Pu, Am L_3-edge $k^3\chi(k)$ EXAFS of Figure 3 for $[An(\alpha\text{-}2\text{-}P_2W_{17}O_{61})_2]^{n-}$ with An^{4+} (Th, U, Np, Pu) and An^{3+} (Np, Pu, Am) in solution and solid forms

An	Th^{4+}	soln −U^{4+}− solid		Np^{4+}	Np^{3+}	Pu^{4+}	Pu^{3+}	Am^{3+}
CN, N_O	8.5(10)	8.4(10)	8.2(10)	8[a]	8[a]	8[a]	8[a]	7.6(10)
Dist., r_{An-O} Å	2.38(1)	2.35(1)	2.33(1)	2.34(2)	2.45(2)	2.33(2)	2.44(2)	2.40(1)
DW, σ^2, Å^2	0.006(1)	0.007(1)	0.008(2)	0.007(1)	0.019(8)	0.006(1)	0.011(2)	0.008(1)
E_0 Shift, eV	3.1(5)	3.0(8)	2.5(8)	5.5(9)	5.5(9)	5.0(9)	4.1(9)	1.7(9)

[a] Fixed parameter.

formed without phase-shift corrections to reveal a single strong peak, due to An−O coordination, as shown in the right panels of Figure 3 (solid lines). There are no other features of physical significance, despite the presence of the distant P and W atoms in the framework structure. The An−O interatomic distances obtained from the curve fitting of the $k^3\chi(k)$ EXAFS are presented in Table 2. The fits to the experimental $k^3\chi(k)$ EXAFS are shown as dashed lines in the left panels of Figure 3. The FTs representing the best fits (dashed lines) exhibit good correspondence with the primary data (solid lines), thereby confirming that the one-shell fits of 8 oxygen atoms adequately describe the An−O coordination in $[An(\alpha\text{-}2\text{-}P_2W_{17}O_{61})_2]^{n-}$ for both An^{3+} and An^{4+} in solution as well as in the solid phase. These results are consistent with the previous EXAFS model for Ln bonding with the monovacant Wells−Dawson anion $[\alpha\text{-}2\text{-}P_2W_{17}O_{61}]^{10-}$,[11] and with the independent work of Bion et al.[4] who have shown that the 8 O environment of U^{4+} is the same for the solid and the solution. The average An−O_8 and Ln−O_8 bond lengths for the $[An(\alpha\text{-}2\text{-}P_2W_{17}O_{61})_2]^{n-}$ and $[Ln(\alpha\text{-}2\text{-}P_2W_{17}O_{61})_2]^{n-}$ series of clusters are presented in Figure 4 as a function of 5*f*- and 4*f*-ionic radii (IR) of Shannon[27] for coordination number (CN) VIII.

The 8 data points for the An-coordinated complexes [Pu^{4+}, Np^{4+}, U^{4+} (solid and solution), Th^{4+}, Am^{3+}, Pu^{3+}, and Np^{3+}] are shown as solid squares in Figure 4(a). There is a linear dependence of the bond lengths from the smallest (Pu^{4+}, IR = 0.960 Å) and highest charge cations to the largest (Np^{3+}, IR = 1.12 Å) and lowest charge ones. The overall increase of the An−O distances with increasing ionic radii is evident from the linear least-squares fit (R^2 = 0.929), which is shown as the solid line in the figure. The slope and intercept are 0.77(9) and 1.58(9) Å, respectively.

The Ln−O distances in the isostructural $[Ln^{3+}(\alpha\text{-}2\text{-}P_2W_{17}O_{61})_2]^{17-}$ and $[Ce^{4+}(\alpha\text{-}2\text{-}P_2W_{17}O_{61})_2]^{16-}$ complexes are plotted against their published eight-coordinate ionic radii[27] in Figure 4(b). The 11 open squares illustrate the systematic increase of the Ln−O distances with the increasing ionic radii of Ce^{4+}, Lu^{3+}, Er^{3+}, Y^{3+}, Dy^{3+}, Tb^{3+}, Gd^{3+}, Eu^{3+}, Nd^{3+}, Pr^{3+}, and Ce^{3+}. The linear least-squares fit (R^2 = 0.949) is shown as the solid line in the figure. The slope, 0.78(6), and intercept, 1.56(6), of this fit are statistically equivalent to those obtained from the fit to the An−O distances of Figure 4(a), suggesting that the An and Ln ions have similar coordination behavior as a function of ionic size.

As with the An and Ln Wells−Dawson butterfly complexes of Figure 1(a), the Lindqvist decatungstate complexes provide an 8 O square antiprism coordination environment, illustrated in Figure 1(b), for both An and Ln cations. In view of the resemblance of the innermost O coordination environments provided by these two polyoxoanions, evaluation of the Lindqvist Ln−O bond length dependence on IR as shown in Figure 4(c) is informative. For the six $[Ln^{3+}(W_5O_{18})_2]^{9-}$ (Ln^{3+} ≡ Dy, Tb, Gd, Sm, Nd, Pr) previously published[18] crystal structures with the same countercations−$K_3Na_4H_2$−there is a linear dependence of bond length with IR. The least-squares fit (R^2 = 0.846) to the 6 distances − open squares in Fig-

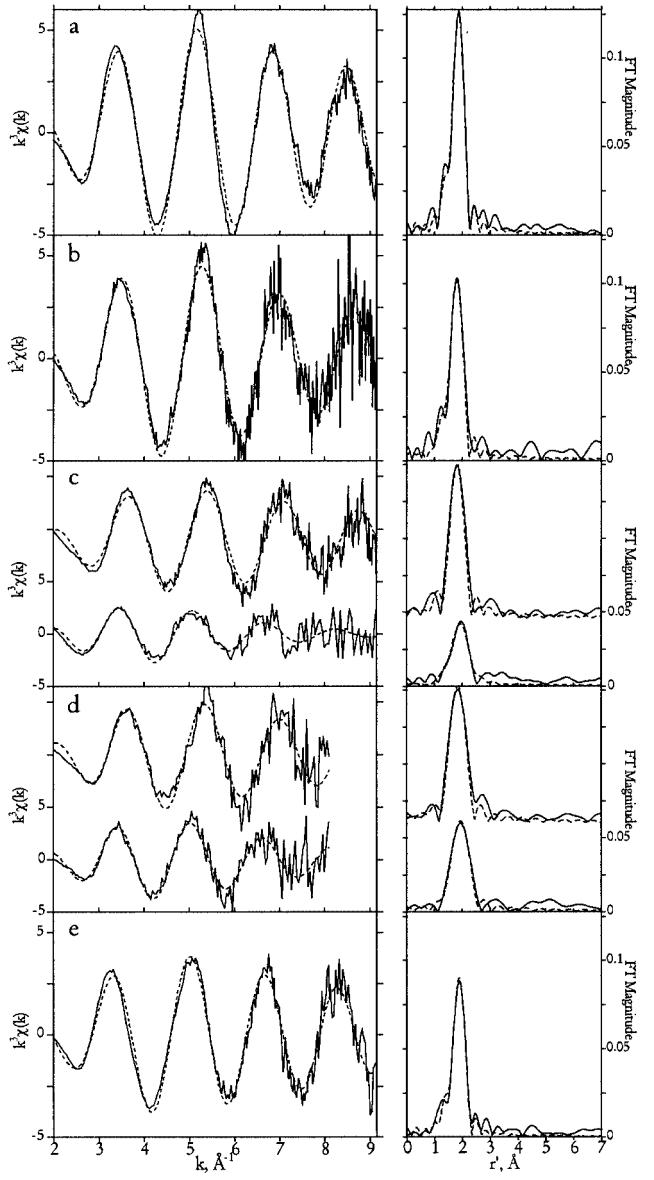

Figure 3. (Left panel) The experimental $k^3\chi(k)$ EXAFS data (solid lines) for $[An(\alpha\text{-}2\text{-}P_2W_{17}O_{61})_2]^{n-}$ with An of (a) Th^{4+}, (b) U^{4+}; (c) Np^{4+} (top) and Np^{3+} (bottom); (d) Pu^{4+} (top) and Pu^{3+} (bottom); (e) Am^{3+}. (Right panel) Fourier transform data (solid lines) of the $k^3\chi(k)$ EXAFS to the immediate left. The best fits are shown as dashed lines in both the Left and Right panels

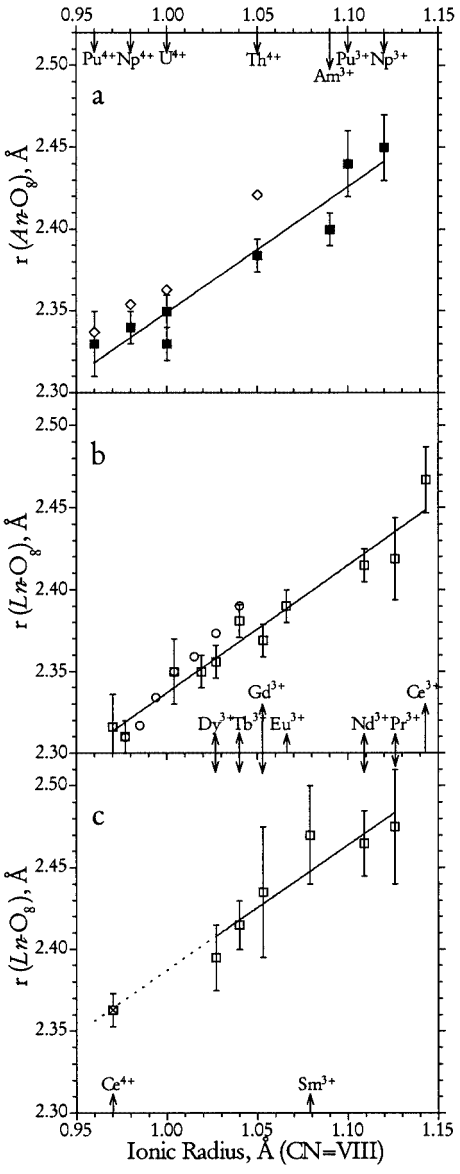

Figure 4. Variation of the $An-O_8$ and $Ln-O_8$ interatomic distances with the appropriate ionic radii of Shannon[27] for CN= VIII. (a) The EXAFS results for the solid K^+ salts and solutions of $[An(\alpha\text{-}2\text{-}P_2W_{17}O_{61})_2]^{n-}$ with An^{3+} and An^{4+} ions (solid squares) and the least-squares fit (solid line). Open diamonds are the $An-O_8$ distances for the AnO_2 solids of Th^{4+}, 2.421(1) Å;[43] U^{4+}, 2.363(1) Å;[44] Np^{4+}, 2.354(1) Å;[45] Pu^{4+}, 2.337(1)[45] Å. (b) The EXAFS-determined $Ln^{n+}-O_8$ distances (open squares) for the solid K^+ salts of $[Ln^{n+}(\alpha\text{-}2\text{-}P_2W_{17}O_{61})_2]^{n-20}$ and the least-squares fit (solid line) with 11 ions (Ce^{4+}, Lu^{3+}, Er^{3+}, Y^{3+}, Dy^{3+}, Tb^{3+}, Gd^{3+}, Eu^{3+}, Nd^{3+}, Pr^{3+}, and Ce^{3+}, in order of increasing IR). The EXAFS-determined distances of Ishiguro et al.[32] for the trivalent aquo ions of Lu−Tb are shown as open circles. (c) The crystallographically-determined average distances of Ozeki et al.[18] for 6 $Na_4K_3H_2[Ln^{3+}(W_5O_{18})_2]$ salts (open squares) and the least-squares fit (solid line), which is extrapolated to the IR for Ce^{4+} (0.97 Å) for comparison with the average crystallographic $Ce^{4+}-O_8$ distance determined for $Na_8[Ce^{4+}(W_5O_{18})_2]$[24]

ure 4(c) − is shown as the solid line, which was extrapolated (dashed line) to the IR minimum (0.96 Å) of Figure 4(a). The soundness of the extrapolation is evident from the coincidence of the crystallographically determined $Ce^{4+}-O$ interatomic distance (square at 0.97 Å) for $[Ce^{4+}(W_5O_{18})_2]^{8-}$.[24] The slope, 0.77(16), and intercept, 1.62(18), of the Ln−O distance vs. IR correlation for the Lindqvist complexes are statistically equivalent with those for the Ln and An Wells−Dawson complexes, thus providing quantitative evidence for the similarity of coordination environments in these two tetradentate polyoxometalate ligands.

Having viewed the Ln- and An−O distances in the context of polyoxometalate structural chemistry, it is informative to gauge the distances of Figure 4(a) and (b) (solid and open squares, respectively) with those for other systems in which Ln and An ions are known to be 8 coordinate with

O atoms. For example, the solid dioxides, AnO_2, are prototypical materials in which all An^{4+} are 8 coordinate. The An−O bond lengths for Pu^{4+}, Np^{4+}, U^{4+}, and Th^{4+} in the AnO_2 fluorite structures are presented in Figure 4(a) as open diamonds. Although these are generally longer than the An−O distances [Figure 4(a), solid squares] for the Wells−Dawson complexes of An^{4+}, they are within agreement in view of the experimental uncertainties, including the 0.04 Å difference between the $[Th(\alpha\text{-}2\text{-}P_2W_{17}O_{61})_2]^{16-}$ and ThO_2 distances.

Comprehensive studies of the $Ln^{3+}\cdot nH_2O$ aquo species indicate that the hydration number (n) is 8 for the small, heavy ions at the end of the 4*f* series, $Tb^{3+}-Lu^{3+}$.[28−31] The Ln−O bond lengths, from the work of Ishiguro et al.,[32] for these 8 coordinate Ln aquo ions is shown in Figure 4(b) (open circles). The bond lengths for the $[Ln(\alpha\text{-}2\text{-}P_2W_{17}O_{61})_2]^{17-}$ complexes [Figure 4(b), open squares] with Tb−Lu ($0.977 \leq IR \leq 1.04$ Å) generally agree with those for the corresponding aquo ion species. In view of the differences in nuclearity and charge between the tetradentate anionic (10−) heteropolyoxometalate and the monodentate neutral water molecule, it is surprising that the bond lengths are so much alike.

Because the large, light Ln^{3+} and An^{3+} ions can assume hydration numbers of 9 or more, there is a dearth of metrical detail for additional systematic comparisons. In fact, the fixed eightfold O coordination for all An/Ln ions in the Wells−Dawson butterfly series of Figure 1(a) may not result in the formation of especially robust complexes with the large Ln^{3+} and An^{3+} compared with the smaller ones, including the tetravalent ions. This view is borne out in the data of Figure 5, which is a plot of the formation constants, $\log\beta_2$, available from the work of Bion et al.[10] versus 1/IR for CN = VIII of Ce^{3+}, Am^{3+}, Eu^{3+}, U^{4+}, Ce^{4+}, and Pu^{4+}. Based upon interpretations of similar plots for other Ln^{3+} complexes,[29,31] the overall direct dependence of $\log\beta_2$ with 1/IR is evidence that the coordination does not change.

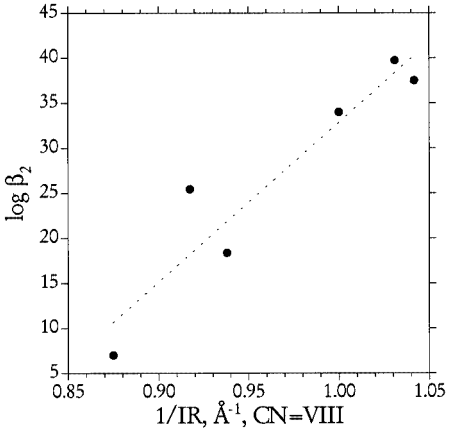

Figure 5. The absolute formation constants, log β_2, of Bion et al.[10] versus 1/IR of Shannon[27] for CN = VIII of the Ce^{3+}, Am^{3+}, Eu^{3+}, U^{4+}, Ce^{4+}, and Pu^{4+} ions (in order of increasing 1/IR) for the Wells−Dawson butterfly complexes of Figure 1(a). The least-squares fit (dashed line, $R^2 = 0.889$) with slope = 177±31 and intercept = −145±30.

Moreover, the regular variation of $\log\beta_2$ with 1/IR indicates similar cation-anion interactions throughout the 4*f*- and 5*f*-series of Wells−Dawson complexes. Although detailed insights are not available with the limited data (six points) of Figure 5, the approximately linear correlation ($R^2 = 0.889$) is consistent with our EXAFS data. The fairly large formation constants of Figure 5 for U^{4+}, Ce^{4+}, and Pu^{4+} are consistent with their short bond lengths and, hence, strong complexation. As expected, the largest ion, Ce^{3+}, of the series in Figure 5, has the smallest formation constant and the longest distance.

The variation of interatomic distances and formation constants with IR, depicted in Figures 4 and 5, show no indication of precipitous changes in An−anion interactions that would account for the stability of the An^{4+} complexes. Instead, a simple electrostatic explanation, arising from ionic charge and size changes, is consistent with all the data in hand. Although the Wells−Dawson and Lindqvist anions stabilize the small An^{4+} ions, this is not general behavior in An and Ln polyoxometalate chemistry. For example, we have found that the Preyssler anion, $[P_5W_{30}O_{110}]^{15-}$, stabilizes Ce^{3+} over Ce^{4+},[33,34] despite the large negative charge on the anion. Tetravalent Ce forms one of the strongest complexes of the Wells−Dawson series, $[Ce(\alpha\text{-}2\text{-}P_2W_{17}O_{61})_2]^{16-}$, but has yet to form a complex with the Preyssler anion.[33,34] Similarly, although Pu^{4+} is stabilized in $[Pu(\alpha\text{-}2\text{-}P_2W_{17}O_{61})_2]^{16-}$, it is Pu^{3+} that is stabilized in $[PuP_5W_{30}O_{110}]^{12-}$.[35] Whereas the present results support the use of the monovacant α-2-$[P_2W_{17}O_{61}]^{10-}$ isomer in the PUREX and SESAME processes for U^{4+} analyses and Am^{4+} valence control, respectively, a predictive understanding of the effects of different polyoxometalates on An redox speciation is not yet available.

Conclusion

The technological prospects of polyoxometalates, in general, and of α-2-$[P_2W_{17}O_{61}]^{10-}$, in particular, for use in radioactive waste processing operations are due to, in part, the strength of their chemical interactions with *f*-elements, particularly the tetravalent 5*f* (actinide) ions. By comparisons with published structures of An dioxides with 8 O coordination environments, we have shown that the $An^{4+}-O$ interactions in complexes of $[An(\alpha\text{-}2\text{-}P_2W_{17}O_{61})_2]^{16-}$ are of the expected magnitude. The variations of An−O interatomic distances and formation constants with An ionic radii are consistent with behavior expected from simple electrostatic considerations of charge and size. Identical behavior was found for $Ln^{3+}-O$ and $Ce^{4+}-O$ coordination in $[Ln(\alpha\text{-}2\text{-}P_2W_{17}O_{61})_2]^{17-}$ and $[Ce(\alpha\text{-}2\text{-}P_2W_{17}O_{61})_2]^{16-}$ as well as for the Lindqvist complex anions, $[Ln^{3+}(W_5O_{18})_2]^{9-}$ and $[Ce(W_5O_{18})_2]^{8-}$. The stability of U^{4+}, Np^{4+}, and Pu^{4+} in complexes $[An(\alpha\text{-}2\text{-}P_2W_{17}O_{61})_2]^{16-}$ and $[An(W_5O_{18})_2]^{8-}$ is understood in terms of strong electrostatic interactions between the spherical An^{4+} cations and the anionic polyoxometalate ligands.

Experimental Section

CAUTION. Th, U, Np, Pu, and Am are radioactive elements. All experiments with these isotopes were performed in specialized laboratories using procedures designed and approved to minimize radiological and chemical hazards. For the transuranic elements, i.e., Np, Pu, and Am, their limited availability, together with radiation exposure concerns, require the use of only mg quantities and thereby limit studies to small sample sizes.

Syntheses: The lacunary, monovacant isomer, $K_{10}[\alpha\text{-}2\text{-}P_2W_{17}O_{61}]\cdot 20H_2O$, was isolated as described elsewhere.[36] The 1:2 $[An(\alpha\text{-}2\text{-}P_2W_{17}O_{61})_2]^{n-}$ complexes with natural Th and U, ^{237}Np, ^{242}Pu, and ^{243}Am were prepared in milligram-scale quantities, by methods adapted from larger-scale syntheses of the lanthanide complexes,[37] through the dropwise addition of one equivalent of Th^{4+}, U^{4+}, Np^{4+}, Pu^{4+}, and Am^{3+} in 1 M $HClO_4$ to warm (60 °C) stirred solutions containing two equivalents of $K_{10}[\alpha\text{-}2\text{-}P_2W_{17}O_{61}]\cdot 20H_2O$ in 0.5 M CH_3CO_2Li buffers of pH = 4.7. The resulting white, violet, yellow, pink, and orange colored solid potassium salts, respectively, were obtained by cooling and slow evaporation of the mother liquor. The An sources were $Th(NO_3)_4\cdot nH_2O$ (Alfa−Aesar); UCl_4 (Strem); purified ^{237}Np stock solution of $[Np(V)O_2]ClO_4$ that was electrochemically reduced to Np^{4+} according to previous procedures;[26,38] purified ^{242}Pu stock solution of $[Pu^{4+}(ClO_4)_4]$ in which the tetravalent oxidation state of Pu was maintained by vigorous sparging with NO; column-purified $^{243}AmCl_3$. The series of 1:2 $[Ln^{3+}(\alpha\text{-}2\text{-}P_2W_{17}O_{61})_2]^{17-}$ complexes for Ce, Pr, Nd, Eu, Gd, Tb, Dy, Y, Er, and Lu as well as $[Ce^{4+}(\alpha\text{-}2\text{-}P_2W_{17}O_{61})_2]^{16-}$ were synthesized and isolated as solid potassium salts in the same manner from $K_{10}[\alpha\text{-}2\text{-}P_2W_{17}O_{61}]\cdot 20H_2O$ and commercial Ln nitrates and Ln chlorides.

Measurements: Aqueous electrolytes consisting of 2:1 v/v mixtures of 0.5 M CH_3CO_2Li buffer at pH = 4.7 and 1 M $HClO_4$ were used for the solution XAFS experiments and in situ bulk electrolyses, which were performed with a BAS 100B/W electrochemical workstation and a purpose-built cell of previous design.[26,39] Carbon rod (Alfa) working and auxiliary electrodes and a Ag/AgCl reference electrode (BAS) were used as described elsewhere.[34] We first collected data for dilute (ca. 1 mM) solutions of $[An^{4+}(\alpha\text{-}2\text{-}P_2W_{17}O_{61})_2]^{16-}$ for An ≡ U, Np, and Pu in the spectroelectrochemical cell with the electrodes at rest potential. This was followed by exhaustive (99−99.9%) electrolysis at −1.00 V and −0.30 V to produce the reduced heteropoly blue species with Np^{3+} and Pu^{3+}, $[An^{3+}(\alpha\text{-}2\text{-}P_2W_{17}O_{61})_2]^{n-}$, that were maintained throughout the data acquisition with the electrode polarized at these potentials. Subsequent oxidation of the heteropoly blues provided X-ray and electrochemical signals that were the same as those for the starting materials, indicating reversibility of the redox chemistry. All XAFS data were obtained at the 7 GeV APS BESSRC CAT station 12 BM-B with a Si<111> monochromator and focusing optics.[40] The An L_3-edge X-ray data were acquired with a multi-element fluorescence detector (Canberra) and the Ln L_3-edge data were acquired with a Lytle-type ion chamber (The EXAFS Co.) in the conventional 45/45° configuration without slits and filters. Energy calibration was maintained with respect to Y metal powder (Th and U L_3-XAFS), Zr foil (Np and Pu L_3-XAFS), and Nb foil (Am L_3-edge XAFS) by setting the inflection points in the first differential transmission XANES data to 17.038, 17.998, and 18.986 eV, respectively. Between four and twelve scans were summed for the solution species and solid samples. XANES and EXAFS data analyses were performed with WinXAS.[41] All EXAFS data were truncated at $k_{max} \approx 9$ Å^{-1} to reduce noise in the FT data and to keep the inner-sphere An−O structural information clear. In view of the range of data available here ($\Delta k \approx 7$ Å^{-1}, $\Delta r \approx 2$ Å^{-1}) and the maximum number of independent parameters ($N_{idp} \approx 8$), we were careful to use conservative models in the curve fitting with single-scattering phase and backscattering amplitude calculations from FEFF8.01.[42] Three or, at most, 4 parameters (O coordination number, N_O; An−O interatomic distance, r; Debye−Waller factor, σ^2; energy shift, ΔE_0) were refined in the single-shell curve fitting with $S_0^2 = 1$.[38]

Acknowledgments

We thank S. Skanthakumar of the Chemistry Division Actinide Facility and the staff of the BESSRC CAT at the Advanced Photon Source for assistance. This work is supported by the U.S. DOE, BES−Chemical Sciences and Material Sciences and, during the initial stages, by sponsorship of the Environmental Management Science Program, Office of Science and Technology, Office of Environmental Management, all under contract No. W-31-109-ENG-38.

[1] A. B. Yusov, V. P. Shilov, *Radiochem., Engl. Transl.* **1999**, *41*, 1−23.
[2] D. E. Katsoulis, *Chem. Rev.* **1998**, *98*, 359−388.
[3] L. Bion, P. Moisy, C. Madic, *Radiochim. Acta* **1995**, *69*, 251−257.
[4] L. Bion, P. Moisy, F. Vaufrey, S. Meot-Reymond, E. Simoni, C. Madic, *Radiochim. Acta* **1997**, *78*, 73−82.
[5] C. Madic, J. Bourges, J.-F. Dozol, *AIP Conf. Proc.* **1995**, *346*, 628−638.
[6] M. Kamoshida, T. Fukasawa, F. Kawamura, *J. Nucl. Sci. Technol.* **1998**, *35*, 185−189.
[7] T. Asakura, L. Donnet, S. Picart, J. M. Adnet, *J. Radioanal. Nucl. Chem.* **2000**, *246*, 651−656.
[8] D. Chartier, L. Donnet, J. M. Adnet, *Radiochim. Acta* **1999**, *85*, 25−31.
[9] An illustration of the structure of $[U^{4+}(\alpha\text{-}2\text{-}P_2W_{17}O_{61})_2]^{16-}$ is provided by A. Müller, F. Peters, M. T. Pope, D. Gatteschi, *Chem. Rev.* **1998**, *98*, 239−271 without presentation of metrical information.
[10] L. Bion, F. Mercier, P. Decambox, P. Moisy, *Radiochim. Acta* **1999**, *87*, 161−166.
[11] Q.-H. Luo, R. C. Howell, M. Dankova, J. Bartis, C. W. Williams, W. D. Horrocks Jr., V. G. Young, A. L. Rheingold, L. C. Francesconi, M. R. Antonio, *Inorg. Chem.* **2001**, *40*, 1894−1901.
[12] V. N. Molchanov, L. P. Kazanskii, E. A. Torchenkova, V. I. Simonov, *Sov. Phys. Crystallogr., Engl. Transl.* **1979**, *24*, 96−97.
[13] I. A. Charushnikova, A. Y. Garnov, N. N. Krot, S. B. Katser, *Radiochem., Engl. Transl.* **1997**, *39*, 424−429.
[14] A. M. Golubev, L. A. Muradyan, L. P. Kazanskii, E. A. Torchenkova, V. I. Simonov, V. I. Spitsyn, *Soviet J. Coord. Chem. Engl. Transl.* **1977**, 715−720.
[15] W. P. Griffith, N. Morley-Smith, H. I. S. Nogueira, A. G. F. Shoair, M. Suriaatmaja, A. J. P. White, D. J. Williams, *J. Organomet. Chem.* **2000**, *607*, 146−155.
[16] T. Ozeki, M. Takahashi, T. Yamase, *Acta Crystallogr., Sect. C: Cryst. Struct. Commun.* **1992**, *C48*, 1370−1374.
[17] T. Ozeki, T. Yamase, *Acta Crystallogr., Sect. C: Cryst. Struct. Commun.* **1993**, *C49*, 1574−1577.
[18] T. Ozeki, T. Yamase, *Acta Crystallogr., Sect. B: Struct. Sci.* **1994**, *B50*, 128−134.
[19] T. Ozeki, T. Yamase, *Acta Crystallogr., Sect. C: Cryst. Struct. Commun.* **1994**, *C50*, 327−330.
[20] M. Sugeta, T. Yamase, *Bull. Chem. Soc., Jpn.* **1993**, *66*, 444−449.

[21] T. Yamase, T. Ozeki, *Acta Crystallogr., Sect. C: Cryst. Struct. Commun.* **1993**, *C49*, 1577−1580.
[22] T. Yamase, T. Ozeki, K. Ueda, *Acta Crystallogr., Sect. C: Cryst. Struct. Commun.* **1993**, *C49*, 1572−1574.
[23] T. Yamase, T. Ozeki, M. Tosaka, *Acta Crystallogr., Sect. C: Cryst. Struct. Commun.* **1994**, *C50*, 1849−1852.
[24] C. Rosu, T. J. R. Weakley, *Acta Crystallogr., Sect. C: Cryst. Struct. Commun.* **1998**, *54*, CIF-access paper IUC9800047.
[25] S. D. Conradson, I. Al Mahamid, D. L. Clark, N. J. Hess, E. A. Hudson, M. P. Neu, P. D. Palmer, W. H. Runde, C. D. Tait, *Polyhedron* **1998**, *17*, 599−602.
[26] L. Soderholm, M. R. Antonio, C. Williams, S. R. Wasserman, *Anal. Chem.* **1999**, *71*, 4622−4628.
[27] R. D. Shannon, *Acta Crystallogr., Sect. A* **1976**, *32*, 751−767.
[28] A. Habenschuss, F. H. Spedding, *J. Chem. Phys.* **1980**, *73*, 442−450.
[29] E. N. Rizkalla, G. R. Choppin, in: *Handbook on the Physics and Chemistry of Rare Earths, Vol. 15* (Eds.: K. A. Gschneidner, Jr, L. Eyring), Elsevier Science, New York, **1991**, pp. 393−442.
[30] C. Cossy, L. Helm, D. H. Powell, A. E. Merbach, *New J. Chem.* **1995**, *19*, 27−35.
[31] H. Kanno, *Mater. Sci. Forum* **1999**, *315−317*, 477−483.
[32] S. Ishiguro, Y. Umebayashi, M. Komiya, *Coord. Chem. Rev.* **2002**, *226*, 103−111.
[33] M. R. Antonio, L. Soderholm, *Inorg. Chem.* **1994**, *33*, 5988−5993.
[34] M. R. Antonio, L. Soderholm, C. W. Williams, N. Ullah, L. C. Francesconi, *J. Chem. Soc., Dalton Trans.* **1999**, 3825−3830.
[35] M. R. Antonio, M.-H. Chiang, C. W. Williams, L. Soderholm, unpublished results **2003**.
[36] R. Contant, *Inorg. Synth.* **1990**, *27*, 104−111.
[37] J. Bartis, S. Sukal, M. Dankova, E. Kraft, R. Kronzon, M. Blumenstein, L. C. Francesconi, *J. Chem. Soc., Dalton Trans.* **1997**, 1937−1944.
[38] M. R. Antonio, L. Soderholm, C. W. Williams, J.-P. Blaudeau, B. E. Bursten, *Radiochim. Acta* **2001**, *89*, 17−25.
[39] M. R. Antonio, L. Soderholm, I. Song, *J. Appl. Electrochem.* **1997**, *27*, 784−792.
[40] M. A. Beno, M. Engbretson, G. Jennings, G. S. Knapp, J. Linton, C. Kurtz, U. Rütt, P. A. Montano, *Nucl. Instrum. Methods Phys. Res. A* **2001**, *467−468*, 699−702.
[41] T. Ressler, *J. Synchrotron Radiat.* **1998**, *5*, 118−122.
[42] J. J. Rehr, R. C. Albers, *Rev. Mod. Phys.* **2000**, *72*, 621−654.
[43] F. Hund, W. Durrwachter, *Z. Anorg. Allg. Chem.* **1951**, *265*, 67−72.
[44] R. E. Rundle, N. C. Baenziger, A. S. Wilson, R. A. McDonald, *J. Am. Chem. Soc.* **1948**, *70*, 99−105.
[45] W. H. Zachariasen, *Acta Crystallogr.* **1949**, *2*, 388−390.

Received January 9, 2003

